Metrol. Meas. Syst., Vol. 25 (2018) No. 3, pp. 617–629.

PAN POLSKA AKADEMIA NAUK

METROLOGY AND MEASUREMENT SYSTEMS

Index 330930, ISSN 0860-8229

www.metrology.pg.gda.pl

M&MS

ANALYSIS OF THE IMPACT OF INTERIOR ORIENTATION PARAMETERS IN DIFFERENT UAV-BASED IMAGE-BLOCK COMPOSITIONS ON POSITIONAL ACCURACY

Dejan Grigillo[1)], Matija Uršič[2)], Matej Bone[3)], Tomaž Ambrožič[1)], Polona Pavlovčič-Prešeren[1)], Mojca Kosmatin-Fras[1)]

1) *University of Ljubljana, Faculty of Civil and Geodetic Engineering, Jamova cesta 2, SI-1000 Ljubljana, Slovenia* (✉ *dejan.grigillo@fgg.uni-lj.si*, +386 1 47 68 654, *tomaz.ambrozic@fgg.uni-lj.si*, *polona.pavlovcic@fgg.uni-lj.si*, *mojca.kosmatin-fras@fgg.uni-lj.si*)

2) *DEZIS d.o.o., Goriška cesta 12, SI-5270 Ajdovščina, Slovenia* (*matija.ursic@dezis.si*)

3) *C-ASTRAL, Tovarniška cesta 26, SI-5270 Ajdovščina, Slovenia* (*matej.bone@c-astral.com*)

Abstract

Understanding the factors that influence the quality of *unmanned aerial vehicle* (UAV)-based products is a scientifically ongoing and relevant topic. Our research focused on the impact of the *interior orientation parameters* (IOPs) on the positional accuracy of points in a calibration field, identified and measured in an orthophoto and a point cloud. We established a calibration field consisting of 20 materialized points and 10 detailed points measured with high accuracy. Surveying missions with a fixed-wing UAV were carried out in three series. Several image blocks that differed in flight direction (along, across), flight altitude (70 m, 120 m), and IOPs (known or unknown values in the image-block adjustment) were composed. The analysis of the various scenarios indicated that fixed IOPs, computed from a good geometric composition, can especially improve vertical accuracy in comparison with self-calibration; an image block composed from two perpendicular flight directions can yield better results than an image block composed from a single flight direction.

Keywords: unmanned aerial vehicle, calibration field, interior orientation parameters, positional accuracy assessment.

1. Introduction

Gathering mass spatial data is traditionally in the domain of remote sensing and photogrammetry. Due to the unprecedented developments of advanced technologies that include imaging sensors, processing and handling large volumes of data, as well as emerging new platforms, we have recently witnessed a vast expansion of applications [1]. The use of *unmanned aerial vehicles* (UAVs) as a platform for data collection has proven to be an especially strong driving force behind the growth in the remote sensing market [1, 2]. A comprehensive review of UAVs applied to 3D mapping is provided in [3]. UAVs are also known under the more general terms such as *unmanned aerial (or aircraft) system* (UAS) or *remotely piloted aerial (or aircraft) system* (RPAS). However, the common user is more familiar with the simpler term "drone". In this

Article history: received on Mar. 20, 2018; accepted on Apr. 22, 2018; available online on Sep. 30, 2018, DOI: 10.24425/123897.

paper, we use the term UAV, because we wish to highlight the platform that enables close-range aerial surveying.

A comprehensive and systematic analysis of UAV-derived product quality is presented in [4]. The results of this research indicate that accurate initial positions and the number and distribution of GCPs are among the main influencing parameters in reducing deformation in the block adjustment process. Another extensive research based on a commonly available dataset (ISPRS/EuroSDR benchmark on multi-platform photogrammetry) investigated the influence of different parameters in oblique airborne image sets [5]. Some researchers investigated the potential of UAV-based photogrammetry and accuracy of the derived products. The positional quality of orthophoto, assessed with various methodologies and used by national mapping agencies, is reported in [6]. The authors have established that the *ground sample distance* (GSD) and the flight's altitude (*above the ground level* – AGL) are important factors which strongly influence the final accuracy of the orthophoto. In [7], a developed UAV-photogrammetry system has been extensively tested for precise modelling of an open-pit gravel mine. A thorough analysis of the influence of different flight parameters on the orthophoto produced for archaeological area surveys is presented in [8]. It was discovered that it is important to achieve a balance between various input parameters; however, the final accuracy is mainly influenced by altitude (AGL). Another investigation of the influence of the image quality on the orthophoto production [9] revealed that images acquired in poor weather conditions reduce the final accuracy of photogrammetric products by an average of 25%. It has been shown that it is important to consider that the error distribution is not normal when assessing the quality of UAV-products, thus robust accuracy measures are more reliable [10]. An overview of the use of UAVs for cultural heritage documentation is given in [11], while an example of the use of UAV photogrammetry in land surveying is presented in [12].

Although the use of UAVs for data collection has many advantages, there are also a few disadvantages. One of them is the payload limitation, which means that we have to use miniature sensors. Most commonly, light consumer-grade digital cameras which are not specially designed for photogrammetric purposes are used for image data acquisition, while small metric cameras that are tailored for high precision UAV applications are still under development and testing [13]. The main disadvantage of the most commonly used cameras lies in instability of their inner geometry over time, thus the term "non-metric camera" is used in association with photogrammetric applications. In addition, small cameras usually employ an electronic rolling shutter readout, which can lead to additional image geometry distortions that are hard to eliminate, especially when flying at higher speeds. An explicit mathematical model that can reduce the effect of a rolling shutter has been developed and tested [14]. The procedures and formulae known from traditional photogrammetry [15] can also be used for UAV flight planning. Some computer programs developed especially for this purpose are freely available from the web (*e.g.* Mission Planner, Tower). When processing UAV-based image blocks, including the generation of sparse point clouds, self-calibration adjustment and the generation of dense point clouds, modern feature extraction and matching methods can be successfully employed [16–18] presents a critical evaluation of commercial packages tested on complex (aerial and terrestrial) datasets acquired with various cameras and platforms.

Within the context of this short review of the current state-of-the-art in this research field, the driving motivation behind our research was to perform some further experiments and analyse their results, so that we could improve our understanding of certain factors that influence the quality of UAV-based products. Our basic research question was: "Is there a significant difference in the image-block adjustment if we use pre-defined IOPs as fixed values or if we compute these parameters as unknowns?"

In order to obtain the best possible control and verification data we have established a calibration field with stabilized and measured geodetic network points of very high accuracy. We performed our surveying missions over the established calibration field in three series, which enabled us to test various scenarios. The image-block compositions treated in our experiments differed in flight direction (along or across), flight altitude (70 m and 120 m above the ground), and IOPs (either as known or unknown values in the image-block adjustment). The results of our experiments are presented numerically and graphically, and their discussion and interpretation are given for each part of the research.

2. Calibration field and geodetic network adjustment

Our goal was to establish a stable calibration test field for long-term use. We chose a 180 m long and 70 m wide test area at a petrol station in Vipava, Slovenia. In total, 20 evenly distributed and visible points for precise geodetic surveying from the ground as well as from an UAV were physically determined (Fig. 1).

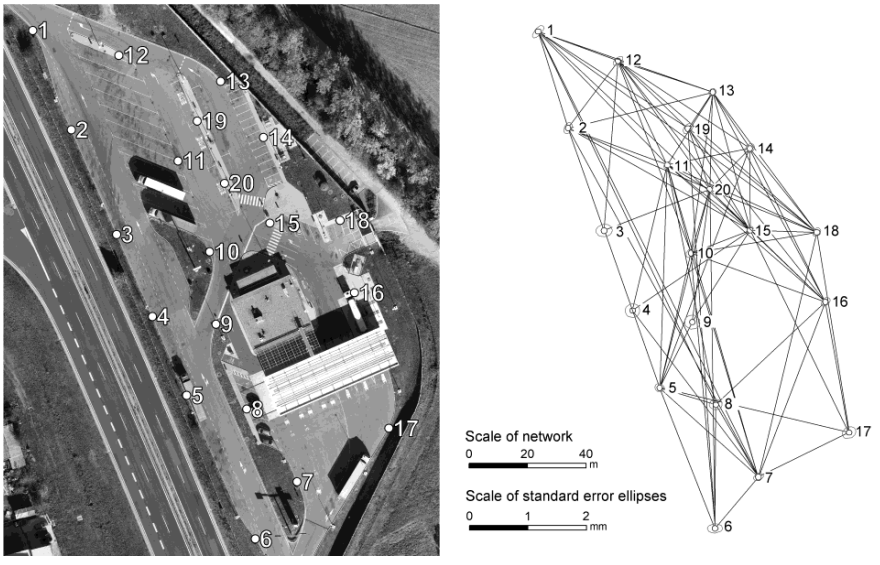

Fig. 1. The calibration field area with the marked locations of 20 stabilized network points that served as GCPs and check points in our research (left). A network sketch and the achieved accuracy of the points' coordinates in the horizontal plane is shown with the standard ellipses of the error (P = 39.4%) (right).

The relative relationship between the points in the calibration field was primarily determined from precise terrestrial measurements. Moreover, GNSS static measurements were performed for five specific points, 1, 6, 9, 13 and 20 (Fig. 1). The GNSS adjusted network coordinates served for the transformation of the remaining points into the Slovene representation of ETRS89. This procedure enabled us to: a) acquire the best possible relations between points (with the use of precise terrestrial measurements), b) determine the coordinates of all points within the global coordinate system, and thus establish the connection between the calibration field and the UAV's flight trajectory. At each specific point terrestrial measurements were performed in four sets of angles with the use of a Leica Geosystems TS30 electronic tachymeter and high precision

accessories [19]. The positions of the points were considered separately for the horizontal plane and the heights. The height differences were obtained by trigonometric levelling.

Due to the lack of known vertical points in the vicinity of the calibration field we used ellipsoidal heights for our study. Redundant height differences from trigonometric levelling followed the free-network adjustment. The final heights of the remaining points were computed by the S-transformation. The results from several sets of known points were eventually compared in order to determine the best set of known points (1, 6 and 13) for the S-transformation. The poorest height accuracy was estimated at 0.3 mm and was related to the point obtained by the intersection of all three axes of the instrument. We can conclude that the final heights of the calibration field were estimated with an accuracy better than 1 mm.

The horizontal network followed the same free-network procedure as regards the use of the corrected distances and mean values of horizontal directions. We estimated a-posteriori standard deviation of 1.4″ for directions and 0.2 mm for distances. The adjustment followed the S-transformation with which we computed the coordinates of the remaining points. As for height adjustment, we acquired very good, maybe even too optimistic standard deviations of the horizontal coordinates (Fig. 1) related to the intersection of the three axes of the instrument. We can conclude that the horizontal coordinates were determined with a submillimetre accuracy.

In order to obtain more check points for evaluating the positional accuracy in our experiments, 10 additional well-defined detail points were surveyed within the calibration field with a precise terrestrial geodetic method.

3. Photogrammetric surveying and image-block compositions

In our research we used a Bramor rTK system, a product developed by C-ASTRAL, which enables long range operation, has a long autonomy and a payload of up to 0.6 kg. It can be used for civil as well as military purposes. The Bramor rTK system consists of a fixed wing UAV, a built-in Sony Alpha 6000 camera, an *inertial navigation system* (INS), a GNSS receiver and data connection, a ground control station with software and a catapult used for take-off. For mission planning and execution we used a dedicated GeoPilot software, also developed by C-ASTRAL. Additionally, Virtual Cockpit (a product developed by Lockheed Martin) was used to operate the vehicle during its mission, as this product also includes necessary safety protocols in the event of forced landing or safety parachute opening.

The photogrammetric image blocks were processed using Agisoft Photoscan, Professional Edition, Version 1.1.6. Using advanced Structure from Motion algorithms, this software enables the adjustment of image blocks and the geo-referencing of images using GCPs as well as generation of photogrammetric point clouds and orthophotos. We used Autodesk Autocad Civil 3D for measuring the horizontal position of the check points in the orthophoto and determining their vertical position in the point cloud for the purpose of the final quality assessment.

In order to verify stability of the IOPs and to experience diverse field conditions that normally occur in projects, we performed our surveying missions on three different days in April, October and November of the same year. These were our three surveying missions (first, second and third).

In each mission, the aerial survey was performed at two different altitudes (AGL 70 m and 120 m), and in two different directions for each altitude: along the shorter side of the block (composition A) and along the longer side of the block (composition B) (Fig. 2). The GSD of the images was 0.91 cm for 70 m, and 1.16 cm for 120 m AGL. The forward overlap of the images

was 75% while the side overlap was 65%. The image-block compositions are given in Table 1. The names of the image blocks are composed from the flying altitude and the flight direction.

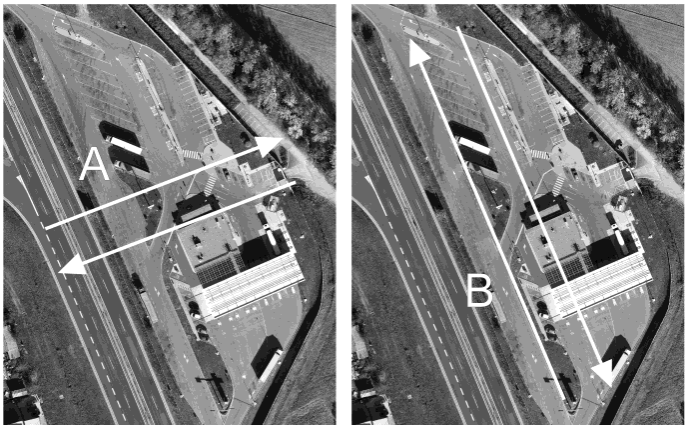

Fig. 2. Flying missions in different flight strip directions: composition A along the shorter side of the block (left) and composition B along the longer side of the block (right).

Table 1. Numbers of flight strips and images for each mission.

IMAGE-BLOCK COMPOSITION	1ST MISSION				2ND MISSION				3RD MISSION			
	70A	70B	120A	120B	70A	70B	120A	120B	70A	70B	120A	120B
Strips in block	5	11	4	6	5	10	4	7	4	11	4	7
Images in block	76	65	36	26	65	53	49	45	52	61	45	38

4. Research methodology, results and discussion

In conventional photogrammetry metric cameras come with a laboratory calibration protocol that provides highly accurate IOPs. On the other hand, in UAV-based photogrammetry the use of low-cost non-metric cameras is usually the only option due to the small payload of the vehicle. In this case, you have to perform your own camera calibration, either prior to or during the project.

There are many quality issues concerning the IOPs of non-metric cameras. The most critical is their instability over time. From this point of view, the best approach would be to compute IOPs during the self-calibration bundle adjustment. However, this method has to meet the following requirements: multi-station convergent imaging networks, fixed zoom/focus and aperture settings, well-defined object points, sufficient variation within the imagery in the scale, comprehensive and unsystematic coverage of the available sensor format, high observational redundancy, adoption of an appropriate and complete camera model [20]. Obviously, it is difficult to meet all of these requirements in UAV missions, thus the quality of IOPs could be vague. Therefore, it might be better to perform camera calibration under good geometric conditions prior to the implementation of the project and to import the IOPs as known values. In order to further improve the self-calibration adjustment results, a two-step camera calibration method is proposed by [21], in which the geometric distortion is removed from the images prior to the adjustment. The correlations between interior orientation parameters using the self-calibration method in close-range

photogrammetry are studied in [22]. Another case when IOPs must be known in advance is when using the UAV-born direct georeferenced photogrammetric platform [23]. On-line and off-line estimation methods of the UAV position based on the measurements from its integrated navigation system are presented in [24].

In our research, we performed various scenarios regarding IOPs, in which we investigated the difference between self-calibrated IOPs and fixed IOPs. As we cannot reach conclusions solely from the precision measurements of the IOPs given in the adjustment report (which is explained in greater detail in [20]), the best approach is to observe the impact different IOPs have on the check points in the final products, in our case the orthophoto and the dense point cloud.

Our investigations were performed in three diverse situations:

– self-calibrated IOPs for selected image-block compositions (Subsection 4.1);
– two sets of fixed IOPs, applied in selected image-block compositions (Subsection 4.2);
– different sets of fixed IOPs, applied in a single image block (Subsection 4.3).

In order to obtain the best possible values of the fixed IOPs, the image blocks were adjusted using all 20 GCPs presented in Fig. 1. In our examples we computed all available IOPs with the applied software [25]: the focal length in x- and y-dimensions measured in pixels, the principal point coordinates, skew and four coefficients of radial and tangential distortion.

In the experiments in which we used self-calibrated or fixed IOPs to evaluate their impact on accuracy of the final products, the image blocks were adjusted using four GCPs (points 2, 6, 13 and 17, see Fig. 1). The 16 remaining GCSs and additional 10 detail points were used as check points. For each particular image-block composition, a dense point cloud was computed from the geo-referenced images with applied image-matching algorithms. Then, a digital surface model in the form of an irregular triangular network was generated from the dense point cloud in order to produce the orthophoto mosaic of the calibration field area.

The assessment of the positional accuracy of the calibration field points in orthophotos and point clouds was methodologically the same in all experiments. The planar coordinates of the check points were manually interpreted and measured in the orthophoto. For the same planar position of a check point, the height was interpolated from the four nearest points in the dense point cloud.

We calculated the differences between the measured coordinates (orthophoto and point cloud) and the ground coordinates, as well as the RMSE values for horizontal (RMSE_{xy}) and vertical accuracy (RMSE_z) for all of the check points (1) to (4).

$$dXY_i = \sqrt{(X_{2i} - X_{1i})^2 + (Y_{2i} - Y_{1i})^2}, \tag{1}$$

$$RMSE_{XY} = \sqrt{\frac{\sum dXY_i^2}{n}}, \tag{2}$$

$$dZ_i = Z_{2i} - Z_{1i}, \tag{3}$$

$$RMSE_Z = \sqrt{\frac{\sum dZ_i^2}{n}}. \tag{4}$$

Expressions in (1) to (4): $(X_{1i}, X_{2i}, Y_{1i}, Z_{1i})$ represent the coordinates of the measured points in the orthophoto (X, Y) and point cloud (Z), (X_{2i}, Y_{2i}, Z_{2i}) are the ground measured coordinates of the same points, n is the number of check points.

4.1. Self-calibration of IOPs for selected image-block compositions

We formed three groups of image blocks for each of the three missions (Table 2). Two additional image blocks were later (see Subsection 4.2) used to calculate the fixed IOPs for the 2nd mission (2_70AB and 2_70AB_120AB), which showed the best results.

Table 2. The selected compositions of image blocks in three missions.

GROUP	1ST MISSION	2ND MISSION	3RD MISSION
1	1_70A	2_70A	3_70A
2	1_70B	2_70B	3_70B
3	1_120A	2_120A	3_120A
		2_70AB	
		2_70AB_120AB	

For each image-block composition presented in Table 2, we computed IOPs as unknowns in the self-calibration adjustment. Following the general work-flow, once an image block was georeferenced, we produced a dense point cloud and an orthophoto. In total, eleven point clouds and eleven orthophotos were produced and RMSE values were computed. The numerical results are given in Table 3 and Table 4, while their graphical presentation can be found in Fig. 3.

Table 3. RMSE values of check points when applying self-calibration in different group compositions.

RMSE Value	Composition 70A			Composition 70B			Composition 120A		
	1	2	3	1	2	3	1	2	3
Horizontal [cm]	2.5	0.9	2.2	1.7	1.5	2.2	3.6	0.9	1.5
Vertical [cm]	10.7	7.9	8.4	5.5	9.6	7.3	12.3	2.0	13.6

Table 4. RMSE values of check points when applying self-calibration in image-block compositions 2_70AB and 2_70AB_120AB.

RMSE Value	Composition	Composition
	2_70AB	2_70AB_120AB
Horizontal [cm]	0.9	0.8
Vertical [cm]	3.5	3.0

When analysing these results, we can notice certain patterns and derive a few conclusions. The horizontal and vertical RMSE values are the lowest in the 2nd mission (except for the vertical RMSE in composition 70B), which was expected as this mission had the best field conditions.

Both image blocks composed of images taken in A and B flight directions (2_70AB and 2_70AB_120AB) achieved better accuracy than any of the image blocks composed merely of a single flight direction (the sole exception is the vertical accuracy of image block 2_120A). However, when comparing image-block compositions 2_70AB and 2_70AB_120AB, the differences of RMSE horizontal and vertical values are very small. Theoretically, we would expect an improvement of accuracy when we have images from different flight altitudes because we obtain a greater variation in the scale, which is desired for good performance of self-calibration [26, 27]. However, our experiment does not show a significant improvement in the results when

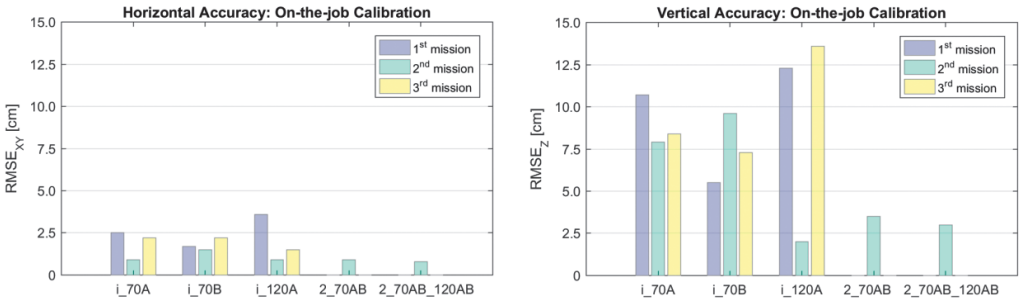

Fig. 3. A graphical presentation of RMSE values when applying the self-calibration approach (*i* denotes the mission number): horizontal RMSE values for check points measured from the orthophoto (left) and vertical RMSE values for check points measured from the dense point cloud (right).

adding images from the flight at an altitude of 120 m. The reason might lie in the fact that the pixel size of the two flight altitudes is almost the same (approximately 1 cm), thus the geometry of image block does not differ considerably. Furthermore, the experimental results in [4], where there was investigated the impact of the flight altitude on the bundle block adjustment accuracy, showed an unexpected deviation from the theoretically calculated vertical accuracy (for 50, 60, 70 and 80 m) which decreases with altitude. However, for a particular type of UAV the accuracy increased with altitude. This is not the same situation as in our experiment, but it indicates that, when using UAVs, the experimental results may differ from the theoretical expectations due to a variety of unpredictable factors that can influence the results, which is not normally the case in traditional photogrammetry. Thus, further and more focused research on UAVs is necessary in order to fully understand the processes.

In general, the first mission has worse results due to the initial problems with the execution of the mission and the high reflectance of the point's surface that resulted in an overexposed image. These problems were solved in time for the second and third missions.

The difference between the flight directions A and B is not distinctive. The same can be said for the various flying altitudes. We can further notice a difference between the horizontal and vertical accuracies which is most probably caused by the fact that we used the minimum of 4 GCPs in the corners of an image block as a ground reference.

4.2. Two sets of fixed IOPs, applied in selected image-block compositions

In order to investigate the difference between self-calibrated IOPs and fixed IOPs we computed two sets of IOPs from image blocks 2_70AB and 2_70AB_120AB, respectively. Each set of computed IOPs was further applied as fixed a-priori values (meaning that IOPs were not computed during the adjustment) in the nine image-block compositions for all three missions presented in Table 3. Again, dense point clouds and orthophotos were produced for each of the image-block compositions, and RMSE values were computed. The results of applying IOPs 2_70AB are given in Table 5, and presented graphically in Fig. 4. The results of applying IOPs 2_70AB_120AB are given in Table 6, and presented graphically in Fig. 5.

From the presented results we can clearly see that – generally speaking (with some exceptions in the 1st mission) – better results are achieved by applying fixed IOPs computed from a better geometric block composition and using a larger number of GCPs (20) in the adjustment.

Table 5. Check point RMSE values when applying fixed IOPs, computed from image-block composition 2_70AB.

RMSE Value	Composition 70A			Composition 70B			Composition 120A		
	1	2	3	1	2	3	1	2	3
Horizontal [cm]	1.7	0.9	2.3	3.9	1.3	1.3	2.9	1.4	1.4
Vertical [cm]	6.6	2.2	5.6	8.6	2.5	4.5	19.4	4.8	3.6

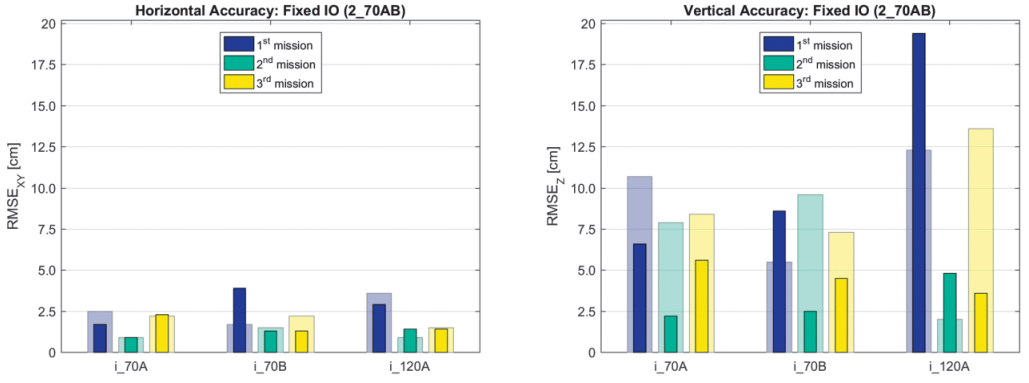

Fig. 4. A graphical presentation of RMSE values when applying fixed IOPs (previously computed from image block 2_70AB) in other image-block compositions, *i* denotes the mission number: horizontal RMSE values for check points measured from the orthophoto (left); vertical RMSE values for check points measured from the dense point cloud (right). The paler bars are RMSE values from the self-calibration (the same as depicted in Fig. 3), added here to visually compare the results.

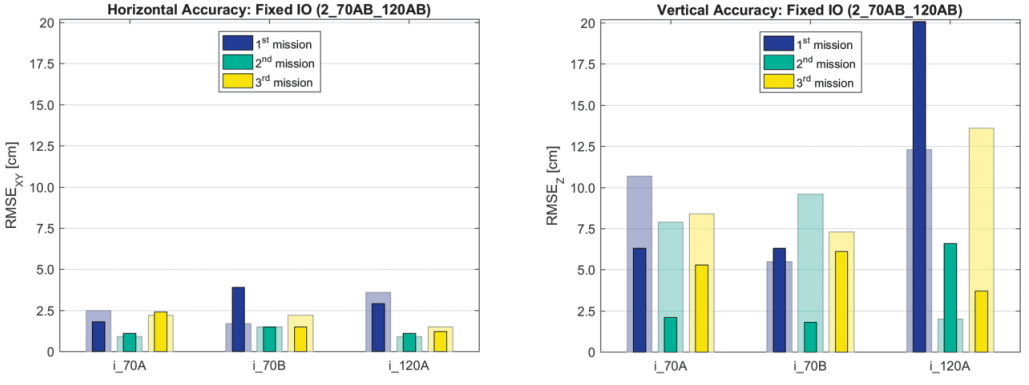

Fig. 5. A graphical presentation of RMSE values when applying fixed IOPs (previously computed from image block 2_70AB) in other image-block compositions, *i* denotes the mission number: horizontal RMSE values for check points measured from the orthophoto (left); vertical RMSE values for check points measured from the dense point cloud (right). The paler bars are RMSE values from the self-calibration (the same as depicted in Fig. 3), added here to visually compare the results.

If we look merely at the results from the 2nd and 3rd missions, the horizontal RMSE values obtained using self-calibrated and fixed IOPs are almost the same, but there is a vast difference in the vertical RMSE values. For example, the vertical RMSE value for image block 2_70A drops from 7.9 cm to 2.2 cm when using fixed IOPs, and for image block 2_70B – from 9.6 cm to

Table 6. Check point RMSE values when applying fixed IOPs, computed from image-block composition 2_70AB_120AB.

RMSE Value	Composition 70A			Composition 70B			Composition 120A		
	1	2	3	1	2	3	1	2	3
Horizontal [cm]	1.8	1.1	2.4	3.9	1.5	1.5	2.9	1.1	1.2
Vertical [cm]	6.3	2.1	5.3	6.3	1.8	6.1	20.1	6.6	3.7

2.5 cm. The exception here is again the image block 2_120A, where we obtained good results already with the use of self-calibrated IOPs.

However, the results from using fixed IOPs computed from image blocks 2_70AB and 2_70AB_120AB do not differ significantly, which is somewhat logical as the RMSE values obtained with the use of self-calibrated IOPs for these two image blocks are almost the same (Table 4).

4.3. Different sets of fixed IOPs applied to single image block

In this part, we present the results of investigating the variations in accuracy of check points when we used different sets of fixed IOPs applied to a single image block. As image block 2_70A showed the best overall results in our previous investigations, we selected this composition for the experiment.

This image block was adjusted several times, each time with another set of fixed IOPs, which were previously calculated from different image-block compositions (as presented in Table 7). Four groups of different image-block compositions were formed, each applied in all three missions. Again, we produced point clouds and orthophotos and calculated RMSE values for each of these 12 situations. The computed RMSE values are given in Table 8, and presented graphically in Fig. 6.

Table 7. Sets of IOPs used in this experiment, calculated from different image-block compositions; *p* indicates that IO parameters computed from a particular image block were used as fixed in the adjustment of image block 2_70A.

GROUP	1ST MISSION	2ND MISSION	3RD MISSION
1	p_1_70A	p_2_70A	p_3_70A
2	p_1_70AB	p_2_70AB	p_3_70AB
3	p_1_70A_120B	p_2_70A_120B	p_3_70A_120B
4	p_1_70AB_120AB	p_2_70AB_120AB	p_3_70AB_120AB

Table 8. Check point RMSE values for different IOPs, applied to image-block composition 2_70A.

RMSE Value	p_70A			p_70AB			p_70A_120B			p_120AB_120AB		
	1	2	3	1	2	3	1	2	3	1	2	3
Horizontal [cm]	1.5	0.9	1.0	1.4	0.9	1.0	1.8	0.9	1.1	1.8	1.1	1.2
Vertical [cm]	3.5	2.4	5.0	9.4	2.2	2.3	7.1	5.1	4.8	13.4	2.1	3.5

When analysing these results, we would like to remind that the time difference between the 1st and 2nd missions was six months, while only one month passed between the 2nd and

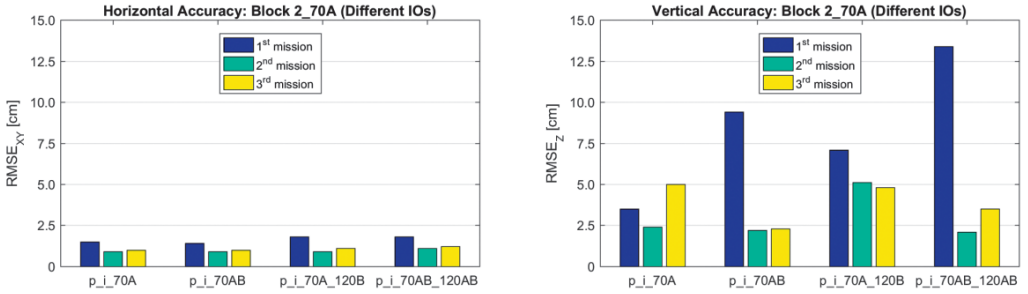

Fig. 6. A graphical presentation of RMSE values when applying fixed IOPs (previously computed from different image-block compositions) in the adjustment of image block 2_70A; *i* denotes the mission number, *p* denotes the origin of applied IO parameters: horizontal RMSE values for check points measured from the orthophoto (left); vertical RMSE values for check points measured from the dense point cloud (right).

3rd missions. This information can be relevant because the IOPs would not remain stable over a longer time span.

What the results of this experiment confirm is that all RMSE values are the lowest for the parameters calculated from the 2nd mission. The results from the 3rd mission differ only slightly, but as expected, the results from the 1st mission are the worst. This would support the assumption regarding the instability of IOPs over time.

For the case of using pre-computed IOPs, the difference in the flight altitude does not seem to have a great influence on the results; the same can be said for a combination of the flight directions, especially regarding the horizontal accuracy. On the other hand, the vertical accuracy is better when using both flight directions, but becomes worse when adding images from the altitude of 120 m.

5. Conclusions

The experiments investigating the impact of different input parameters and compositions in close-range aerial image blocks, using UAV platforms and systems, are very complex and time-consuming. In the presented research we processed numerous image blocks and produced a great number of orthophotos and point clouds with which we investigated the accuracy in various scenarios.

We obtained very accurate ground truth data with a high precision geodetic network as we wanted to exclude any possible doubts in the ground points' accuracy.

Although we prepared the execution plan with utmost care, its performing was not always optimal. We carried out our tests over three different missions in which the field conditions could not be completely the same (*e.g.* weather conditions, light conditions). We discovered that the 1st mission was not performed in the best way, which is clearly reflected in the results. The lesson learned from this case is that it is very important to plan and execute the project in the best possible conditions.

However, certain general conclusions can be reached when we analyse the positional accuracy of the check points in the orthophotos and the point clouds produced from a variety of image-block compositions. The compositions of an image block in both A (along the shorter side of the block) and B (along the longer side of the block) flight directions resulted in greater accuracy of the orthophoto and point cloud than that of image blocks composed solely from a single flight direction.

In most cases using fixed IOPs, computed from a good image-block composition, slightly improved the horizontal accuracy and significantly improved the vertical accuracy (compared with self-calibration). On the other hand, we also confirmed that using IOPs that were calculated closer to the time of the treated image block, led to better results. However, the instability of IOPs through time is an issue that still needs to be investigated in greater detail. Our experiments do not allow us to reach any definite conclusions regarding this issue.

Performing this kind of experiments and interpreting the results is always limited to a certain degree. There are many factors throughout the work-flow that influence the final accuracy. Nevertheless, we believe that the results and conclusions from our experiments contribute to a better understanding of the impact of particular issues in the production and processing of UAV-based image blocks and its products, and can be taken into account in everyday projects.

Acknowledgements

This research was partially founded by the Slovenian Research Agency within the frame of the research program P2-0227(A), Geoinformation Infrastructure and Sustainable Spatial Development of Slovenia.

References

[1] Toth, C., Jóźków, G. (2016). Remote sensing platforms and sensors: A survey. *ISPRS J. Photogramm. Remote Sens.*, 115, 22–36.

[2] Colomina, I., Molina, P. (2014). Unmanned aerial systems for photogrammetry and remote sensing: A review. *ISPRS J. Photogramm. Remote Sens.*, 92, 79–97.

[3] Nex, F., Remondino, F. (2014). UAV for 3D mapping applications: a review. textitAppl. Geomat., 6(1), 1–15.

[4] Nasrullah, A.R. (2016). *Systematic Analysis of Unmanned Aerial Vehicle (UAV) Derived Product Quality*. M.Sc. Thesis. Faculty of Geo-Information Science and Earth Observation of the University of Twente, Enschede, The Netherlands.

[5] Gerke, M., Nex, F., Remondino, F., Jacobsen, K., Kremer, J., Karel, W., Hu, H., Ostrowski, W. (2016). Orientation of oblique airborne image sets – experiences from the ISPRS/EuroSDR benchmark on multi-platform photogrammetry. *ISPRS – Int. Arch. Photogramm. Remote Sens. Spat. Inf. Sci.*, XLI-B1, 185–191.

[6] Mesas-Carrascosa, J.F., Rumbao, C.I., Berrocal, A.J., Porras, G.A. (2014). Positional Quality Assessment of Orthophotos Obtained from Sensors Onboard Multi-Rotor UAV Platforms. *Sensors*, 14(12), 22394–22407.

[7] Shahbazi, M., Sohn, G., Théau, J., Menard, P. (2015). Development and Evaluation of a UAV-Photogrammetry System for Precise 3D Environmental Modeling. *Sensors*, 15(11), 27493–27524.

[8] Mesas-Carrascosa, F.J., Notario García, D.M., Meroño de Larriva, E.J., García-Ferrer, A. (2016). An Analysis of the Influence of Flight Parameters in the Generation of Unmanned Aerial Vehicle (UAV) Orthomosaicks to Survey Archaeological Areas. *Sensors*, 16(11), 1838–1851.

[9] Wierzbicki, D., Kedzierski, M., Fryskowska, A. (2015). Assessment of the Influence of UAV Image Quality on the Orthophoto Production. *Int Arch Photogramm Remote Sens Spat. Inf Sci*, XL-1/W4, 1–8.

[10] Kosmatin Fras, M., Kerin, A., Mesarič, M., Peterman, V., Grigillo, D. (2016). Assessment of The Quality of Digital Terrain Model Produced from Unmanned Aerial System Imagery. *Int Arch Photogramm Remote Sens Spat. Inf Sci*, XLI-B1, 893–899.

[11] Remondino, F., Stylianidis, E. (2016). Cultural Heritage Documentation with RPAS/UAV. In *3D Recording, Documentation and Management of Cultural Heritage*, Stylianidis, E., Remondino, F., Eds. Dunbeath: Whittles Publishing, 369–379.

[12] El Meouche, R., Hijazi, I., Poncet, P.A., Abunemeh, M., Rezoug, M. (2016). UAV Photogrammetry Implementation to Enhance Land Surveying, Comparisons and Possibilities. *Int Arch Photogramm Remote Sens Spat. Inf Sci*, XLII-2/W2, 107–114.

[13] Kraft, T., Geßner, M., Meißner, H., Cramer, M., Gerke, M., Przybilla, H.J. (2016). Evaluation of a Metric Camera System Tailored for High Precision UAV Applications. *Int Arch Photogramm Remote Sens Spat. Inf Sci*, XLI-B1, 901–907.

[14] Vautherin, J., Rutishauser, S., Schneider-Zapp, K., Choi, H.F., Chovancova, V., Glass, A., Strecha, C. (2016). Photogrammetric Accuracy and Modeling of Rolling Shutter Cameras. *ISPRS Ann Photogramm Remote Sens Spat. Inf Sci*, *III-3*, 139–146.

[15] Kraus, K. (2007). *Photogrammetry, Geometry from Images and Laser Scans*. 2nd ed. Berlin: Walter de Gruyter.

[16] Lingua, A., Marenchino, D., Nex, F. (2009). Performance Analysis of the SIFT Operator for Automatic Feature Extraction and Matching in Photogrammetric Applications. *Sensors*, 9(5), 3745–3766.

[17] Kerner, S., Kaufman, I., Raizman, Y. (2016). Role of Tie-Points Distribution in Aerial Photography. *Int Arch Photogramm Remote Sens Spat. Inf Sci*, XL-3/W4, 41–44.

[18] Remondino, F., Nocerino, E., Toschi, I., Menna, F. (2017). A critical review of automated photogrammetric processing of large datasets. *ISPRS – Int. Arch. Photogramm. Remote Sens. Spat. Inf. Sci.*, XLII-2/W5, 591–599.

[19] Leica Geosystems Carriers. *http://leica-geosystems.com/en/products/gnss-systems/accessories/carriers*. (Aug, 2017).

[20] Luhmann, T., Fraser, C., Maas, H.G. (2016). Sensor modelling and camera calibration for close-range photogrammetry. *ISPRS J. Photogramm. Remote Sens.*, 115, 37–46.

[21] Gašparović, M., Gajski, D. (2016). Two-step Camera Calibration Method Developed for Micro UAV's. *Int Arch Photogramm Remote Sens Spat. Inf Sci*, XLI-B1, 829–833.

[22] Tang, R., Fritsch, D. (2013). Correlation Analysis of Camera Self-Calibration in Close Range Photogrammetry. *Photogramm. Rec.*, 28(141), 86–95.

[23] Chiang, K.W., Tsai, M.L., Chu, C.H. (2012). The Development of an UAV Borne Direct Georeferenced Photogrammetric Platform for Ground Control Point Free Applications. *Sensors*, 12(7), 9161–9180.

[24] Kaniewski P., Gil R., Konatowski S. (2017). Estimation of UAV Position with Use of Smoothing Algorithms. *Metrol. Meas. Syst.*, 24(1), 127–142.

[25] Agisoft PhotoScan User Manual, Professional Edition, Version 1.2. *http://www.agisoft.com/pdf/photoscan-pro_1_2_en.pdf*. (Feb. 2016).

[26] Luhmann, T., Robson, S., Kyle, S., Boehm, J. (2014). *Close-Range Photogrammetry and 3D Imaging*. 2nd ed. Berlin/Boston: Walter de Gruyter.

[27] Tang, R. (2013). *Mathematical methods for camera self-calibration in photogrammetry and computer vision*. Ph.D. Thesis. University of Stuttgart, Germany.